Research Article Vol. 36, No. 7 / July 2019 / Journal of the Optical Society of America B E9

Journal of the Optical Society of America B

OPTICAL PHYSICS

Shaping and polarizing fluorescence emission of a polycrystalline organic semiconductor film by plasmonic nanogratings

Dominik A. Gollmer,[1,2] Christopher Lorch,[1] Frank Schreiber,[1] Dieter P. Kern,[1] and Monika Fleischer[1,3]

[1]Institute for Applied Physics and Center for Light-Matter Interaction, Sensors and Analytics LISA+, Eberhard Karls Universität Tübingen, Auf der Morgenstelle 10 and 15, 72076 Tübingen, Germany
[2]e-mail: dominik.gollmer@uni-tuebingen.de
[3]e-mail: monika.fleischer@uni-tuebingen.de

Received 9 January 2019; revised 23 February 2019; accepted 23 February 2019; posted 25 February 2019 (Doc. ID 357264); published 25 March 2019

The fluorescence emission properties of hybrid systems consisting of a one-dimensional gold nanowire grating and an evaporated thin film of the small molecule organic semiconductor diindenoperylene (DIP) are investigated. The optical properties of the metallic systems are dominated by their plasmonic resonances. The spectral positions of the resonances are tuned through the width of the single nanowires. Additionally, the plasmonic gratings show a strong polarization dependency due to their one-dimensionality. In contrast, the pure organic system has a polarization-independent emission between 570 and 900 nm when excited with blue light, whereas no photoluminescence can be detected from the bare plasmonic system for the same illumination conditions. For the hybrid system, the intensity, the shape of the emission spectrum, and the polarization of the emission clearly correlate with the optical properties of the plasmonic nanowires. Depending on the optical properties of the plasmonic system, different emission bands of the organic thin film can be enhanced.

https://doi.org/10.1364/JOSAB.36.0000E9

1. INTRODUCTION

The optical properties of plasmonic nanostructures have been investigated thoroughly in recent years [1–3]. The resonant excitation of plasmonic nanostructures leads to a strong and localized near-field at their surfaces [2]. Through this associated near-field, localized surface plasmons can couple to adjacent materials and vice versa [4,5]. Thus, in hybrid systems with fluorescent molecules or quantum dots, plasmonic nanostructures can enhance and spectrally shape the spontaneous emission [5–8]. For quantum dots or fluorophores, the polarizability and directionality of the fluorescence emission by plasmonic nanoantennas has been demonstrated [9–11]. Nevertheless, there is still a lack of studies with fluorescence materials suitable for applications. In the present study, a small molecule organic semiconductor is combined with a plasmonic nanowire system. Such organic semiconductors have already been used in several applications like organic solar cells or organic light emitting devices [12,13]. The organic material used in this study is the small molecule organic semiconductor diindenoperylene (DIP) [14]. This organic semiconductor shows good chemical stability and a good structural order when evaporated under ultra-high vacuum conditions and has a strong optical anisotropy [14,15]. Its fluorescence properties and the decay dynamics of excited states in this material have already been investigated in several studies [16–19]. In contrast, only few studies with plasmonic nanostructures and DIP are available, where metal nanotips were employed for local luminescence enhancement or spherical plasmonic nanostructures for excitation enhancement [20,21]. In this work, the emission properties of a hybrid system consisting of an extended one-dimensional (1D) plasmonic nanowire grating and a thin layer of DIP are investigated. DIP is very well-suited for this study since its different emission bands offer strong spectral overlap with the resonances of the plasmonic system. The hybrid system shows a polarized fluorescence emission, which is associated with the optical properties of the plasmonic nanostructures. Additionally, the enhancement of either specific emission bands of DIP or a more broadband enhancement by the plasmonic nanogratings is demonstrated. In contrast to the mentioned previous studies, the present system exhibits fluorescence enhancement that clearly occurs predominantly due to the emission enhancement in a DIP/plasmonic hybrid system and not due to excitation enhancement. The results

shown here are valuable, e.g., for the design of plasmonic nanostructures for light extraction from organic light emitting diodes (OLEDs) [22,23].

2. MATERIALS AND METHODS

A. Sample Fabrication

As the substrate, a glass coverslip (thickness ∼160 μm) is used and coated with 50 nm indium tin oxide (ITO) as a conductive film by magnetron sputtering (20 W, 3×10^{-3} mbar). The gold nanogratings are fabricated by electron beam lithography, thermal evaporation, and lift-off [25 μm × 25 μm arrays, period 400 nm, line width 41–101 nm as determined by scanning electron microscopy (SEM), height 20 nm] [24]. In Fig. 1(b), a SEM image of a grating without DIP is shown. After fabricating the gratings, the organic semiconductor film is deposited in an ultra-high vacuum chamber by thermal evaporation via organic molecular beam epitaxy [25]. The nominal thickness of the organic film is 20 nm. A model of the DIP molecule on the grating is shown in Fig. 1(a). The DIP molecule exhibits a pronounced optical anisotropy, where the dielectric tensor is dominated by the contribution parallel to the long molecule axis [14,26]. Comparing the weighting of the different absorption bands from the spectra in the above-mentioned earlier studies with the results of an extinction spectrum of the pure DIP film on the glass/ITO substrate (not shown), the DIP film seems to be dominated by molecules in an upright formation, with an angle of ∼17° between the long molecule axis and the surface normal. The size of the in-plane domains of the polycrystalline film is much smaller than the investigated spot size, such that their influence on the fluorescence is negligible.

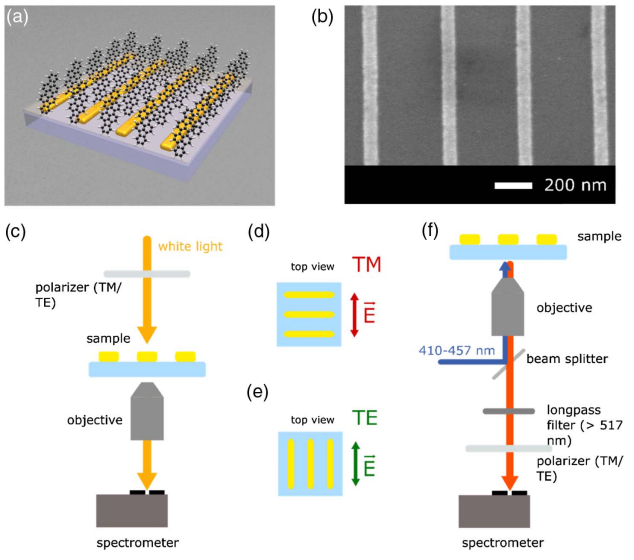

Fig. 1. (a) Schematic of a grating sample with DIP (not to scale). (b) SEM image of the grating with a period of 400 nm and a line width of 74 nm. (c) Schematic of the setup for the extinction measurements with incident polarized white light. (d) and (e) Orientation of the electric-field vector relative to the nanowires for TM and TE polarization in the illumination light path (extinction) or detection light path (fluorescence). (f) Schematic of the setup for the fluorescence measurements with illumination (410–457 nm) and detection (>517 nm) from below.

B. Optical Measurements

The setups for the extinction and fluorescence measurements are shown schematically in Figs. 1(c) and 1(f). For both measurements, an inverted microscope (Nikon Ti-U Eclipse) is used. For the extinction measurements, the gratings are illuminated by collimated white light from a halogen lamp. The light can be polarized through a broadband polarizer in the illumination light path. A 20× objective (NA 0.5) is used for detecting the transmitted light. In the image plane, a pinhole with a diameter of 200 μm is used to select the light from a specific area (diameter 10 μm) on the sample. This light is coupled into the spectrometer. The extinction spectra are calculated by $I_{ext} = 1 - (T/T_{ref})$, where T is the transmission at the position of the gratings with DIP or the substrate with the DIP film, and T_{ref} is a reference transmission spectrum through a glass/ITO substrate without DIP. Figures 1(d) and 1(e) show the orientation of the electric field of the incoming light in the extinction setup, which is oriented perpendicular to the nanowires for transverse magnetic (TM) polarization and parallel to the nanowires for transverse electric (TE) polarization.

For the fluorescence measurements, the sample is illuminated from below through the 20× objective by a mercury lamp (Nikon Intensilight) with unpolarized light (410–457 nm). The emitted light from the sample is detected in reflection, again through the 20× objective. For all fluorescence spectra, the integration time is the same (10 s). A long pass filter is positioned in the detection light path, so only light with a wavelength >517 nm can pass the filter. The detected light is spatially filtered in the image plane, as in the extinction measurements, and coupled into the spectrometer.

In front of the spectrometer entrance, a polarizer is positioned for analyzing the detected light. Please note that here the polarizer is introduced in the detection light path, whereas, for the extinction measurements, the polarizer is placed in the illumination light path. For the fluorescence measurements, the electric-field vectors of TM- and TE-polarized emitted light are oriented in the same way as for the extinction measurements. The transmission properties of the long pass filter lead to a modulation of the transmitted intensity above 720 nm. The characteristics of the filter are therefore determined using white light, and the fluorescence spectra are corrected for these transmission properties.

3. RESULTS AND DISCUSSION

In Fig. 2, the unpolarized fluorescence of a 20 nm thick DIP film on a glass/ITO substrate is shown together with the fluorescence of a hybrid system consisting of the same DIP film on a Au nanowire grating with a period of 400 nm and wire width of 88 nm. Additionally, the response of a comparable bare grating without DIP and the fluorescence of only the glass/ITO substrate are shown when illuminated by the mercury lamp. The DIP shows a strong fluorescence for wavelengths larger than 550 nm. The broad peak around 700 nm may consist of several overlapping emission bands. The spectral positions of the observed emission bands of the pure DIP are comparable with results of previous studies [16–18,20,21]. When comparing the fluorescence of the DIP and the hybrid system, considerable enhancement of about 60% of the unpolarized

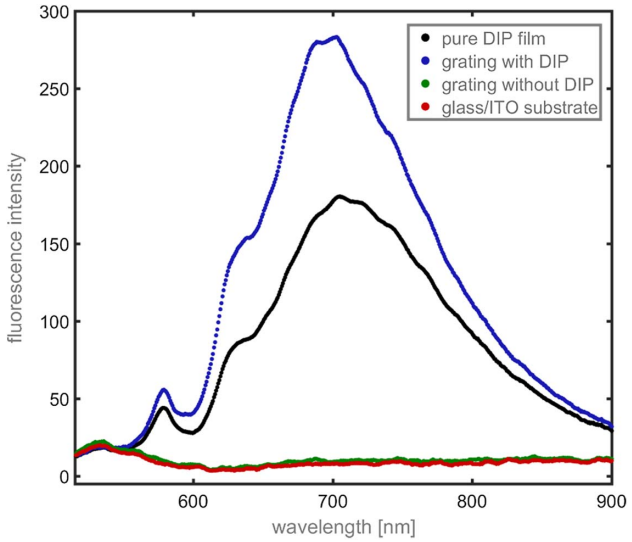

Fig. 2. Unpolarized fluorescence spectra of a DIP film on a glass/ITO substrate (black), of the DIP film on a Au nanowire grating (blue, wire width 88 nm), of a grating without DIP (green), and of the glass/ITO substrate (red).

fluorescence and a slight spectral shift (∼15 nm) of the maximum to shorter wavelengths is visible.

The fluorescence of the bare glass/ITO substrate and of the substrate with a Au nanowire grating do not show any differences, indicating that the bare Au system does not contribute any intrinsic fluorescence. Both systems show a weak emission for wavelengths below 600 nm, but nearly zero emission in the range of the emission of DIP between 600 and 850 nm. Therefore, the fluorescence of the DIP clearly dominates in the hybrid system, whereas the fluorescence of the substrate and the plasmonic system can be neglected.

In Fig. 3, the polarization-dependent emission of the hybrid system measured with the fluorescence setup from Fig. 1(f) is shown for nanowire gratings that each have a period of 400 nm, but different line widths from 41 to 101 nm. For TM-polarized emission, the fluorescence intensity of the grating-coupled system amounts to up to twice the intensity of the pure DIP film at the wavelength of maximum emission near 700 nm. The shape of the fluorescence curves clearly depends on the width of the single Au nanowires. The spectral position of the maximum visibly shifts to longer wavelengths for widths from 74 to 101 nm. The strongest emission occurs for a wire width of 88 nm. For a width of 63 nm, the enhancement of the DIP band at about 630 nm is much more pronounced, whereas only weak homogeneous fluorescence enhancement can be observed for a wire width of 41 nm.

For TE polarization, a slight enhancement of the emission (factor ∼1.2) in the hybrid system compared to the pure DIP fluorescence can be observed for all wire widths. However, in contrast to the results for TM polarization, almost no dependence on the different wire widths is visible.

For further analysis, the TM emission spectra of the hybrid system are normalized by the emission of the 20 nm thick DIP film. The resulting spectrally resolved fluorescence

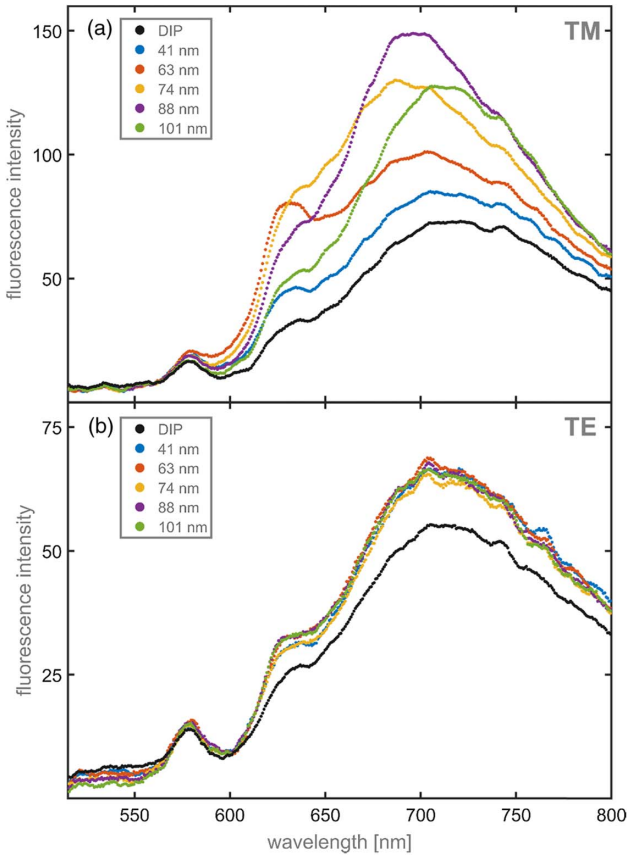

Fig. 3. TM- and TE-polarized emission spectra of the DIP film on glass/ITO substrate (pure DIP) and the DIP film on the nanogratings with different widths of the single wires of 41 to 101 nm when illuminated with the light of wavelengths between 410 and 457 nm. For TM-polarized emission, different enhanced intensities and a shift of the wavelength position of the maximum for increasing wire widths are clearly visible, whereas, for TE-polarized emission, hardly any differences in intensity appear between the wire widths.

enhancement is shown in Fig. 4(a). They are juxtaposed to the extinction spectra of the same gratings with DIP as measured under illumination with TM-polarized white light in the setup from Fig. 1(c), which are shown in Fig. 4(b). The resonances in the extinction spectra, which are attributed to the localized surface plasmon resonances (LSPRs) of the transversely excited Au wires, are clearly visible. Typical TE- and TM-polarized extinction spectra of pure Au gratings can be found in Ref. [27] for comparison.

Additionally, the extinction spectra of the gratings with and without DIP film are simulated using the finite element method (COMSOL Multiphysics) and show a similar behavior as the experimental results (see Fig. 5). The Au lines are defined as a two-dimensional (2D) primitive cell with periodic boundary conditions, cf. Ref. [27], and their widths are chosen to match the experiments. A semi-infinite half-space of glass with a 50 nm ITO layer is defined as the substrate. For the simulations with DIP, a thin film with a thickness of 20 nm is added in the simulations. A wavelength-dependent tensor according to Ref. [14] is used for the refractive index of DIP. The maxima in the extinction spectra shift to longer

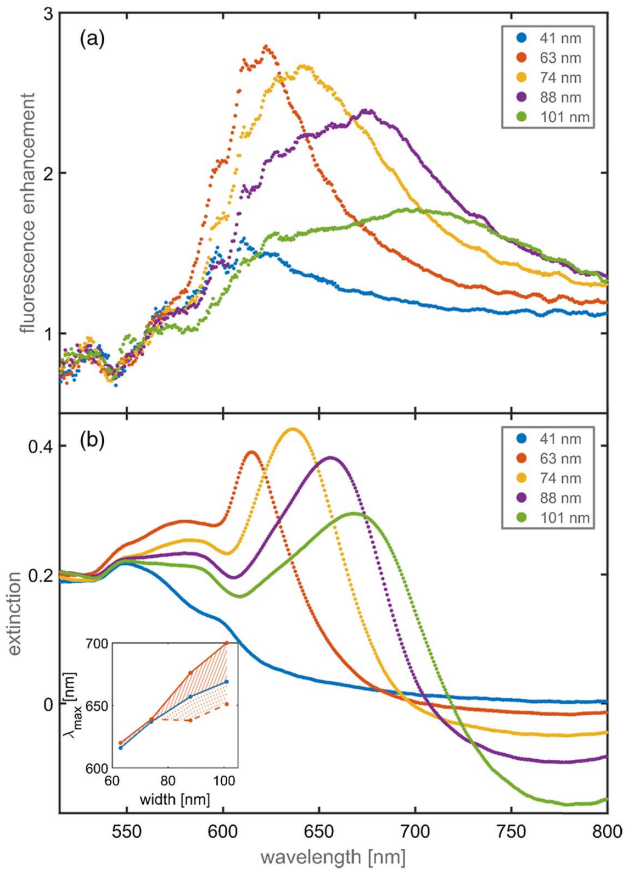

Fig. 4. (a) TM-polarized emission of the different hybrid systems normalized to the emission of the DIP film. (b) White light extinction spectra for TM-polarized incident light for the different wire widths from 41 to 101 nm. Inset: shift of the maxima of the extinction curves (blue line) and the fluorescence enhancement (solid orange line) with increasing wire width. Additionally, the shift of the left shoulder of the fluorescence enhancement peak for Au wire widths of 88 and 101 nm is shown (dashed orange line).

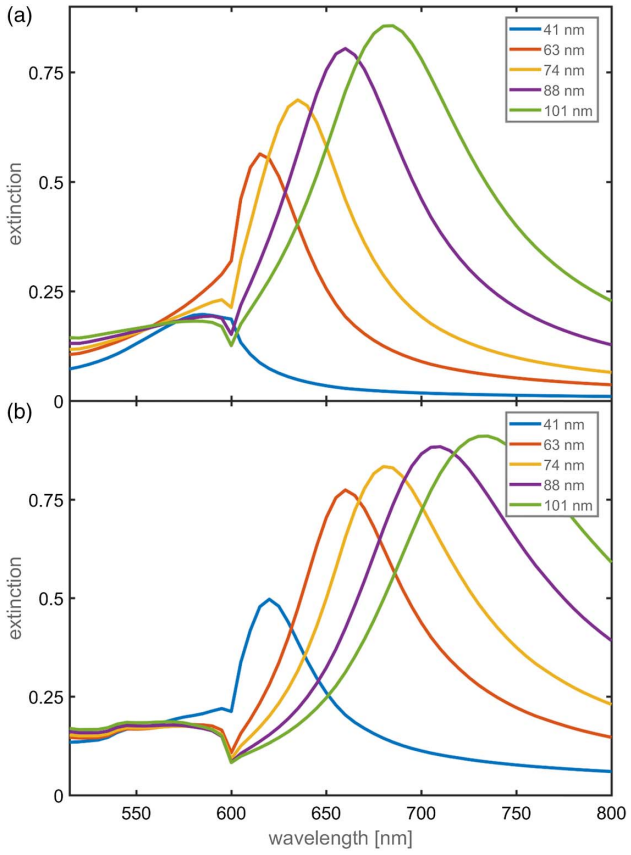

Fig. 5. Simulated extinction spectra of the nanogratings (a) without and (b) with DIP film. The plasmonic resonances, which are spectrally shifting with the wire width, as well as the grating induced sharp dip near 600 nm, are clearly visible.

wavelengths and become broader for increasing linewidths as expected and also seen in the simulations (see Fig. 5). An opposite trend is visible for different heights but fixed width of the lines, with the maxima shifting to longer wavelengths for decreasing heights due to an increasing lateral aspect ratio, as tested in simulations for heights from 15 to 30 nm (not shown). Additionally, near 600 nm, the lattice mode is visible as a dip [28,29]. This mode occurs when the first grating order on the substrate side becomes evanescent at this wavelength (period 400 nm * refractive index ~1.5) [28]. The appearance as a dip and not as a peak here is connected to its spectral position at a larger energy than the LSPR [28–31].

In contrast to the other wire widths, for the width of 41 nm, no clear LSPR in the extinction spectrum is visible in Fig. 4(b). This behavior may be explained by the size of the wires, which leads to a low polarizability [32]. On the other hand, it can be ascribed to a coincidence between the supposed LSPR wavelength near 600 nm and the lattice mode, which may lead to a damping and a resulting very weak resonance. The partly negative values and the tilt of the extinction curves (larger values at smaller wavelengths than at larger wavelengths) can be explained by spectrally dependent antireflection effects due to the effective refractive index of the grating structure when comparing the system with a grating to the glass/ITO reference spectrum, as calculated in the extinction measurements (see Section 2.B).

For all wire widths, the maximum of the fluorescence enhancement appears close to the maximum of the extinction spectra (Fig. 4). It is shifted in a similar way for the extinction maxima and the fluorescence enhancement maxima, as shown in the inset of Fig. 4, for Au lines from 63 to 101 nm in width. For widths of 63 and 74 nm, the wavelengths of the maxima nearly coincide. For widths of 88 and 101 nm, the fluorescence peak seems to split, and, besides the main maximum, a shoulder in the fluorescence enhancement spectra is also visible due to the emission band at 620 nm. The shift of this shoulder is illustrated as a dashed line in the inset of Fig. 4. With these structures, both fluorescence emission bands seem to be enhanced (see also inset of Fig. 4). Additionally, the width of the resonance curves increasingly broadens for the extinction spectra and the fluorescence enhancement spectra with increasing Au wire width. For the extinction spectra, the FWHM increases from ~20 nm for a wire width of 63 nm to ~50 nm for a wire width of 101 nm. For the fluorescence enhancement curves, the corresponding values amount to ~40 nm (wire

width 63 nm) to 130 nm (wire width 101 nm). Note that for both the maxima and the widths of the curves, one does not expect an exactly identical behavior for the extinction and the fluorescence, because the maximum and the width of each fluorescence enhancement spectrum in Fig. 4(a) is influenced by both the fluorescence spectrum of the DIP film and the particular LSPR. A maximum relative emission enhancement is found for the wire width of 63 nm at 622 nm (factor of 2.8), which is slightly stronger than the enhancement for the wires with 74 nm width at 642 nm. The strongest overall integrated fluorescence signal was found for the wire width of 88 nm with a maximum at 697 nm [Fig. 3(a)], whereas, for the 101 nm wires, a weaker, but very broadband enhancement, was found. The smallest structures (width 41 nm) clearly show the weakest enhancement. For wavelengths smaller than 550 nm for all wire widths, a weak attenuation of the fluorescence can be observed, which may be connected to the absorption properties of Au in this wavelength range [33]. Note that the results of the TM-polarized fluorescence only show emission enhancement that can be related to the LSPR of the single nanowires. No apparent enhancement effects from grating induced modes with small bandwidths are observed, in contrast to other reports [34–36]. This can be explained by the grating geometry and the respective spectral position of grating induced effects, as discussed above [28].

Several mechanisms can lead to the fluorescence enhancement in the hybrid system: the increase of light absorption by the DIP molecules due to the enhanced near-field at the surface of the plasmonic nanostructures, changes of the radiative and non-radiative transition rates induced by the metal nanostructures, and/or the coupling of the nanostructures' near-field to the far-field [6,7,37,38]. Because of the unpolarized excitation in the fluorescence setup, a potential absorption effect should be visible in both the TE- and TM-polarized emission data (Fig. 3). Besides other effects, such as the modification of radiative and non-radiative transition rates due to the presence of a metal interface, the coupling of the excited states to propagating plasmons along the nanowires, or an enhancement due to the corrugated interface [39,40], the absorption effect may lead to the weak geometry-independent fluorescence enhancement also visible for TE polarization (Fig. 3). The weakness of this enhancement may be due to the off-resonant excitation of the plasmonic nanostructures in the fluorescence setup. The excitation in the fluorescence setup at 410–457 nm ranges clearly below the wavelengths of the LSPRs (Fig. 4). For TM-polarized emission, the normalized fluorescence is obviously modified by the plasmonic properties of the single nanowires (Fig. 4). Here, the coupling of the molecular fluorescence to the plasmonic modes and the out-coupling via the plasmon modes seems to dominate the optical properties of the hybrid system. This leads to comparable trends for the plasmonic and the normalized fluorescence properties for different wire widths, as shown in Fig. 4. Due to the modification of the local density of optical states by the plasmon resonance and the antenna properties of the plasmonic nanostructures, the fluorescence in the hybrid system appears to be increased [4,5,7,37,38]. For the wires with 63 and 74 nm widths, the left shoulder of the broad fluorescence curve of DIP at around 630 nm is most strongly enhanced (Fig. 4). This region corresponds to an intrinsic fluorescence emission band of DIP with a short decay time [18]. The enhancement of this band leads to the strongest enhancement factors for the system investigated here. For the wire widths of 88 and 101 nm, the emission band near 700 nm, which originates from long-lived states in DIP thin films [18], is more strongly enhanced, but smaller overall enhancement factors are observed (Fig. 4). The smaller enhancement factors for larger line widths may be related to a trade-off between a less strong increase of transition rates and the more efficient out-coupling of plasmon modes for increasing structure sizes, as shown in a theoretical study on nanospheres [37]. This means the respective emission bands, which can be related to certain fluorescence states [18], show different coupling properties within the hybrid system.

Overall, the results presented here show clear evidence for the coupling between small molecule organic semiconductor fluorescence and localized plasmon modes of a metal grating. In the fluorescence curves of the hybrid system for TM polarization, the signature of the plasmonic properties is clearly visible.

In further experiments, time and polarization-dependent measurements could be used for further investigation of the change of the transition rates and decay channels due to the metallic grating [7,38]. With such measurements, the lifetime modification due to the change of the local electromagnetic density of states can be investigated. Additionally, potentially varying lifetime changes for the different emission bands can be examined, which may enable the study of coupling effects for different emission bands [16,18]. Thus, the well-defined hybrid system presented here can act as a model system for fundamental investigations of fluorescence properties in hybrid systems.

4. CONCLUSION

We investigated the fluorescence properties of a hybrid system consisting of a plasmonic nanowire grating and an organic semiconductor thin film. The results are compared with the linear optical properties of the plasmonic system. The fluorescence of the hybrid system is enhanced compared to the fluorescence of the pure DIP film. The fluorescence spectra of the hybrid system clearly correlate with the far-field optical properties of the single Au nanowires and show a partially polarized and enhanced fluorescence emission. The fluorescence properties of the hybrid system arise from a coupling between the fluorescence of the molecules and the LSPR of the single nanowires. The maximum of the fluorescence emission is shifted to longer wavelengths and broadened with increasing wire width. Preferential enhancement of specific emission bands by gratings with different wire widths can be observed. The results have important implications for applications such as broadband light extraction from OLEDs, since with a specific wire width a broadband emission enhancement from 575 to 850 nm can be achieved. For future studies, the system is well-suited for fundamental time-dependent investigations of fluorescence in hybrid organic small molecule/plasmonic systems.

Funding. Baden-Württemberg Stiftung (OPV001); Carl-Zeiss-Stiftung; European Cooperation in Science and Technology (COST).

Acknowledgment. The authors declare that there are no conflicts of interest related to this article.

REFERENCES

1. M. A. El-Sayed, "Some interesting properties of metals confined in time and nanometer space of different shapes," Acc. Chem. Res. **34**, 257–264 (2001).
2. P. Mühlschlegel, H. J. Eisler, O. J. F. Martin, B. Hecht, and D. W. Pohl, "Resonant optical antennas," Science **308**, 1607–1609 (2005).
3. C. Schäfer, D. A. Gollmer, A. Horrer, J. Fulmes, A. Weber-Bargioni, S. Cabrini, P. J. Schuck, D. P. Kern, and M. Fleischer, "A single particle plasmon resonance study of 3D conical nanoantennas," Nanoscale **5**, 7861–7866 (2013).
4. Y. Sugawara, T. A. Kelf, J. J. Baumberg, M. E. Abdelsalam, and P. N. Bartlett, "Strong coupling between localized plasmons and organic excitons in metal nanovoids," Phys. Rev. Lett. **97**, 266808 (2006).
5. P. Anger, P. Bharadwaj, and L. Novotny, "Enhancement and quenching of single-molecule fluorescence," Phys. Rev. Lett. **96**, 113002 (2006).
6. S. Kühn, U. Håkanson, L. Rogobete, and V. Sandoghdar, "Enhancement of single-molecule fluorescence using a gold nanoparticle as an optical nanoantenna," Phys. Rev. Lett. **97**, 017402 (2006).
7. A. J. Meixner, R. Jäger, S. Jäger, A. Bräuer, K. Scherzinger, J. Fulmes, S. zur Oven-Krockhaus, D. A. Gollmer, D. P. Kern, and M. Fleischer, "Coupling single quantum dots to plasmonic nanocones: optical properties," Faraday Discuss. **184**, 321–337 (2015).
8. J. Fulmes, R. Jäger, A. Bräuer, C. Schäfer, S. Jäger, D. A. Gollmer, A. Horrer, E. Nadler, T. Chassé, D. Zhang, A. J. Meixner, D. P. Kern, and M. Fleischer, "Self-aligned placement and detection of quantum dots on the tips of individual conical plasmonic nanostructures," Nanoscale **7**, 14691–14696 (2015).
9. H. Mertens, J. S. Biteen, H. A. Atwater, and A. Polman, "Polarization-selective plasmon-enhanced silicon quantum-dot luminescence," Nano Lett. **6**, 2622–2625 (2006).
10. T. Ming, L. Zhao, Z. Yang, H. Chen, L. Sun, J. Wang, and C. Yan, "Strong polarization dependence of plasmon-enhanced fluorescence on single gold nanorods," Nano Lett. **9**, 3896–3903 (2009).
11. A. G. Curto, G. Volpe, T. H. Taminiau, M. P. Kreuzer, R. Quidant, and N. F. van Hulst, "Unidirectional emission of a quantum dot coupled to a nanoantenna," Science **329**, 930–933 (2010).
12. S. R. Forrest, "Ultrathin organic films grown by organic molecular beam deposition and related techniques," Chem. Rev. **97**, 1793–1896 (1997).
13. J. Wagner, M. Gruber, A. Hinderhofer, A. Wilke, B. Bröker, J. Frisch, P. Amsalem, A. Vollmer, A. Opitz, N. Koch, F. Schreiber, and W. Brütting, "High fill factor and open circuit voltage in organic photovoltaic cells with diindenoperylene as donor material," Adv. Funct. Mater. **20**, 4295–4303 (2010).
14. U. Heinemeyer, R. Scholz, L. Gisslén, M. I. Alonso, J. O. Ossó, M. Garriga, A. Hinderhofer, M. Kytka, S. Kowarik, A. Gerlach, and F. Schreiber, "Exciton-phonon coupling in diindenoperylene thin films," Phys. Rev. B **78**, 085210 (2008).
15. A. C. Dürr, F. Schreiber, M. Münch, N. Karl, B. Krause, V. Kruppa, and H. Dosch, "High structural order in thin films of the organic semiconductor diindenoperylene," Appl. Phys. Lett. **81**, 2276–2278 (2002).
16. M. Heilig, M. Domhan, and H. Port, "Optical properties and morphology of thin diindenoperylene films," J. Lumin. **110**, 290–295 (2004).
17. M. Aghamohammadi, A. Fernández, M. Schmidt, A. Pérez-Rodríguez, A. R. Goñi, J. Fraxedas, G. Sauthier, M. Paradinas, C. Ocal, and E. Barrena, "Influence of the relative molecular orientation on interfacial charge-transfer excitons at donor/acceptor nanoscale heterojunctions," J. Phys. Chem. C **118**, 14833–14839 (2014).
18. V. M. Nichols, K. Broch, F. Schreiber, and C. J. Bardeen, "Excited-state dynamics of diindenoperylene in liquid solution and in solid films," J. Phys. Chem. C **119**, 12856–12864 (2015).
19. M. Hänsel, V. Belova, A. Hinderhofer, F. Schreiber, K. Broch, and P. Tegeder, "Ultrafast excited state dynamics in diindenoperylene films," J. Phys. Chem. C **121**, 17900–17906 (2017).
20. D. Zhang, U. Heinemeyer, C. Stanciu, M. Sackrow, K. Braun, L. E. Hennemann, X. Wang, R. Scholz, F. Schreiber, and A. J. Meixner, "Nanoscale spectroscopic imaging of organic semiconductor films by plasmon-polariton coupling," Phys. Rev. Lett. **104**, 056601 (2010).
21. D. Zhang, A. Horneber, J. Mihaljevic, U. Heinemeyer, K. Braun, F. Schreiber, R. Scholz, and A. J. Meixner, "Plasmon resonance modulated photoluminescence and Raman spectroscopy of diindenoperylene organic semiconductor thin film," J. Lumin. **131**, 502–505 (2011).
22. K. Saxena, V. K. Jain, and D. S. Mehta, "A review on the light extraction techniques in organic electroluminescent devices," Opt. Mater. **32**, 221–233 (2009).
23. W. H. Koo, S. M. Jeong, F. Araoka, K. Ishikawa, S. Nishimura, T. Toyooka, and H. Takezoe, "Light extraction from organic light-emitting diodes enhanced by spontaneously formed buckles," Nat. Photonics **4**, 222–226 (2010).
24. D. A. Gollmer, F. Walter, C. Lorch, J. Novák, R. Banerjee, J. Dieterle, G. Santoro, F. Schreiber, D. P. Kern, and M. Fleischer, "Fabrication and characterization of combined metallic nanogratings and ITO electrodes for organic photovoltaic cells," Microelectron. Eng. **119**, 122–126 (2014).
25. A. Hinderhofer and F. Schreiber, "Organic-organic heterostructures: concepts and applications," ChemPhysChem **13**, 628–643 (2012).
26. U. Heinemeyer, K. Broch, A. Hinderhofer, M. Kytka, R. Scholz, A. Gerlach, and F. Schreiber, "Real-time changes in the optical spectrum of organic semiconducting films and their thickness regimes during growth," Phys. Rev. Lett. **104**, 257401 (2010).
27. D. A. Gollmer, C. Lorch, F. Schreiber, D. P. Kern, and M. Fleischer, "Enhancing light absorption in organic semiconductor thin films by one-dimensional gold nanowire gratings," Phys. Rev. Mater. **1**, 054602 (2017).
28. A. Christ, T. Zentgraf, J. Kuhl, S. G. Tikhodeev, N. A. Gippius, and H. Giessen, "Optical properties of planar metallic photonic crystal structures: experiment and theory," Phys. Rev. B **70**, 125113 (2004).
29. A. Vitrey, L. Aigouy, P. Prieto, J. M. García-Martín, and M. U. González, "Parallel collective resonances in arrays of gold nanorods," Nano Lett. **14**, 2079–2085 (2014).
30. B. Auguié and W. L. Barnes, "Collective resonances in gold nanoparticle arrays," Phys. Rev. Lett. **101**, 143902 (2008).
31. Y. Francescato, V. Giannini, and S. A. Maier, "Plasmonic systems unveiled by Fano resonances," ACS Nano **6**, 1830–1838 (2012).
32. U. Kreibig and M. Vollmer, *Optical Properties of Metal Clusters* (Springer, 1995).
33. P. B. Johnson and R. W. Christy, "Optical constants of the noble metals," Phys. Rev. B **6**, 4370–4379 (1972).
34. G. Vecchi, V. Giannini, and J. Gómez Rivas, "Surface modes in plasmonic crystals induced by diffractive coupling of nanoantennas," Phys. Rev. B **80**, 201401 (2009).
35. V. Giannini, G. Vecchi, and J. Gómez Rivas, "Lighting up multipolar surface plasmon polaritons by collective resonances in arrays of nanoantennas," Phys. Rev. Lett. **105**, 266801 (2010).
36. G. Lozano, D. J. Louwers, S. R. K. Rodriguez, S. Murai, O. T. A. Jansen, M. A. Verschuuren, and J. Gómez Rivas, "Plasmonics for solid-state lighting: enhanced excitation and directional emission of highly efficient light sources," Light: Sci. Appl. **2**, e66 (2013).
37. H. Mertens, A. F. Koenderink, and A. Polman, "Plasmon-enhanced luminescence near noble-metal nanospheres: comparison of exact theory and an improved Gersten and Nitzan model," Phys. Rev. B **76**, 115123 (2007).
38. J. Li, A. V. Krasavin, L. Webster, P. Segovia, A. V. Zayats, and D. Richards, "Spectral variation of fluorescence lifetime near single metal nanoparticles," Sci. Rep. **6**, 21349 (2016).
39. W. L. Barnes, "Fluorescence near interfaces: the role of photonic mode density," J. Mod. Opt. **45**, 661–699 (1998).
40. F. Emmanuel and G. Samuel, "Surface enhanced fluorescence," J. Phys. D **41**, 013001 (2008).